International Journal of Microwave and Wireless Technologies

cambridge.org/mrf

Radiation pattern synthesis of smart fourth dimensional beamforming antenna arrays using optimally splitting pulses

Avishek Chakraborty[1], Ravi Shankar Saxena[2], Indrasen Singh[3], Asha Rajiv[4], Johar Mgm[5], Navdeep Prashar[6], Ashish Singh[7], Sanjeev Kumar Shah[8], Jyoti Bansal[9], Alaa Salim Abdalrazzaq[10], Mustafa Asaad Rasol[11], Sumit Gupta[12] and Durbadal Mandal[13]

[1]Department of Electrical, Electronics and Communication Engineering (EECE), GITAM (Deemed To Be University), Bengaluru, KA, India; [2]Department of Electronics and Communication Engineering (ECE), GMR Institute of Technology (GMRIT), Rajam, AP, India; [3]School of Electronics Engineering, Vellore Institute of Technology, Vellore, TN, India; [4]Department of Physics & Electronics, School of Sciences, JAIN (Deemed to Be University), Bangalore, KA, India; [5]Management and Science University, Shah Alam, Malaysia; [6]Department of Electronics and Communication Engineering (ECE), Chandigarh College of Engineering, Chandigarh Group of Colleges, Jhanjeri, Mohali, Punjab, India; [7]Department of Electrical, Electronics and Vehicle Engineering, NIMS Institute of Engineering and Technology, NIMS University Rajasthan, Jaipur, India; [8]Department of Electronics and Communication Engineering (ECE), Uttaranchal Institute of Technology, Uttaranchal University, Dehradun, India; [9]Department of Electrical and Electronics Engineering, IES College of Technology, IES University, Bhopal, India; [10]Department of Dentistry, Al-Noor University College, Nineveh, Iraq; [11]College of Dentistry, National University of Science and Technology, Dhi Qar, Iraq; [12]Department of Electronics and Communication Engineering (ECE), SR University, Warangal, India and [13]Department of Electronics and Communication Engineering (ECE), NIT Durgapur, West Bengal, India

Research Paper

Cite this article: Chakraborty A *et al*. (2025) Radiation pattern synthesis of smart fourth dimensional beamforming antenna arrays using optimally splitting pulses. *International Journal of Microwave and Wireless Technologies* **17**(3), 455–470. https://doi.org/10.1017/S175907872510158X

Received: 7 August 2024
Revised: 23 March 2025
Accepted: 4 May 2025

Keywords:
beamforming; Sideband radiations (SRs); sidelobe; smart antenna; time modulation

Corresponding author: Avishek Chakraborty; Email: avishekdreamz@gmail.com

Abstract

Designing and developing smart antennas with adaptive radiation characteristics is an integral part for present-day communication systems. The versatile capabilities of Time-modulated fourth-dimensional (4D) antenna arrays can provide that crucial adaptability if properly designed. This work discusses an effective analysis of 4D antenna arrays to achieve less-attenuating radiation patterns with simultaneously suppressed sidelobe and sidebands. The 4D arrays offer an additional benefit over standard arrays in the sense that the requisite amplitude tapering to lower the undesired radiations can be accomplished by controlling only the switch ON times of the radiating elements instead of using attenuators. The idea of splitting pulses by keeping the total switch ON durations constant, is exploited here as an additional degree of freedom for beamforming of all the radiation patterns. The unwanted radiations in terms of sidelobes as well as sideband radiations (SRs) at the fundamental and harmonic frequencies, respectively are simultaneously minimized to improve the radiation efficiencies of the 4D array. To address the conflicting aims for the synthesis of radiation patterns, a wavelet-mutation based heuristic method is also proposed. The multi-objective problem in hand is modulated in to a single objective cost function as minimization problem. The proposed outcomes are reported and compared with other state of the art works related to the same domain. Furthermore, a detailed statistical analysis is also provided to identify the strengths and weaknesses of the proposed approach.

Introduction

Modern communication requires smart antenna arrays with adaptive radiation characteristics. The synthesis of fourth-dimensional (4D) time-modulated antenna arrays have drawn an abundance of attention from the scientific community lately for its adaptive nature [1]. To add a further degree of control to the already existing classic antenna arrays, fourth dimension "time" had been proposed for pattern synthesis [2]. Excitation, phase, and the distance between elements used to be the three dimensions to control the radiation pattern of traditional array. This fourth dimension provided an advantage when the idea of regulating the array patterns by rapid switches had been introduced for electronic scanning [3]. Due to its simple control by switching ON and OFF the antennas, the 4D arrays have emerged as an alternate to tapered phased arrays for achieving ultra-low sidelobe levels (SLLs) [4]. However, the benefit comes with an intrinsic limitation of sideband pattern generation at infinite number of harmonic frequencies, typically thought of as power loss [5]. Since then, so many efforts have been made to synthesize adequate average patterns at antenna operating frequency to reduce the spurious harmonic or sideband

© The Author(s), 2025. Published by Cambridge University Press in association with The European Microwave Association.

radiation (SR) [6–8]. To further improve the efficiency of the array, simultaneous suppression of SLL and minimization of all higher-order sideband levels (SBLs) have been addressed [9, 10]. An alternative strategy for direction finding has also emerged, one that utilizes the SBLs rather than suppressing them [11]. In addition, a novel electronic steering technique was put forth in [12] by controlling the SRs. The 4D arrays had further been investigated to estimate the directions of arrival of target signal [13] by exploiting the beamforming capabilities of the harmonics [14]. The harmonics have also been controlled by moving the phase center of the linear 4D arrays with suitable time schemes [15, 16]. Novel methods to regulate the beam patterns have been made feasible by the design of proficient switching mechanisms utilizing pulse shifting [17] and pulse splitting [18]. Pattern generation of 4D arrays by attenuating [19] or exploiting [20] the SRs has been reported for multifunction radars [21, 22]. Controlling a sideband by progressive phase shifted switching [23], or multiple higher-order sidebands by optimal phase shifting [24, 25] have opened up the possibilities for multipoint communication. Due to its adaptiveness, 4D arrays exhibit multifold prospect compared to its traditional counterparts if the sideband power is properly controlled [26]. Automatic beam steerable 4D arrays with single and multiple steered beams have also come into the picture by channelizing the sideband power in desired directions [27, 28]. The 4D planar arrays have further been proposed for harmonic beamforming [29], and for directional modulation purposes by controlling its phase time sequences [30]. For more advanced applications like monopulse radars, sum-difference beams have also been generated using convex optimization methods [31]. Due to its efficient beamforming capabilities, 4D arrays have also been extensively investigated for physical secure communication [32, 33]. Multi-tone harmonics of 4D arrays have also been explored for Wireless Information and Power Transfer (WIPT) [34]. The harmonics have been used advantageously for steerable energy patterns [35]. Different structures and combinations such as spiral [36], circular and concentric circular [37, 38] and concentric ring shaped 4D antenna arrays [39] have also been tested. Further, the concept had also been applied for Unmanned aerial vehicles and 5 G communications [40, 41]. In this way, time-modulation has become a serious research interest for the modern-world communication [42].

This article contributes to the competitive world of antenna array research by aiming to design an efficient beamforming array with optimal radiation properties. The efficient analysis of 4D linear arrays is discussed in this study to generate less-attenuating radiation patterns with sequentially suppressed sidelobe and sidebands. In this regard, an idea of splitting pulses while maintaining an optimal total switch ON duration is designed as an additional level of freedom for beamforming. In order to improve the overall radiation efficiencies of the array, the SLL and SBLs at the fundamental and harmonic frequencies are minimized. A set of linear arrays containing 16, 24, and 30 elements are investigated by proposing unique splitting pulse switching sequences for each array. Pulse splitting in between optimal modulation period provides an extra edge of control over the undesired radiations and power wasted in higher-order harmonics. The optimal pulse splitting schemes are designed by a wavelet-mutation based heuristic method by taking multiple objectives in a single-objective cost function as minimization problem. The outcomes are compared with other state of the art works, and a detailed statistical analysis is also reported to show the efficacies of the method.

The idea and methods proposed here have numerous benefits over other contemporary methods pertaining to antenna arrays employed for complex beamforming applications. The methodologies proposed in this research, stands out from other contemporary research works, and the advantages or benefits of the proposed methodologies are as follows:

Methodologies: First of all, optimal splitting pulse sequences are designed for efficient beamforming purposes. Second, ultra-low SLLs have been targeted by channelizing maximum power to the main beams. Then, unwanted SBLs have been suppressed to reduce the power wastage and improve efficiencies. This automatically mitigates the unwanted interferences coming from non-desired directions. In addition to that, all the higher sidebands are also lowered and up to 20 SBLs have been reported. For the overall optimization process, wavelet mutation is implemented to balance the exploration and exploitation stages. It is further compared with other hybrid and traditional mutation processes in terms of outcomes of the problem in hand. Finally, simultaneous mitigation of SLLs and SBLs have been proposed by implementing a single beamforming network (BFN).

Benefits: The array is targeted to perform both SLL and SBL reduction simultaneously compared to only SLL reduction or only SBL reduction aimed in most of the other research works. The modulation periods are managed and controlled with optimally splitting pulses in comparison to optimized time duration only reported in most other literature. The splitting pulse concept is also beneficial for BFNs as the optimal radiation properties can be implemented with only one BFN instead of different BFNs used to control the main beam and side beams separately reported in other works. Thus, only one BFN is sufficient here for both SLL and SBL reduction and simplifies the implementational task compared to its counterparts. As the proposed work is free from BFN related implementational complexities, it also provides an adaptive, robust, and efficient method of beamforming compared to the conventional ones. The performance of the beamforming arrays has also improved to a large extent due to wavelet mutation-based heuristic optimization methods employed to determine the optimal duration and ON-time instants.

The sequence of the remaining material is as follows: The design insights and the switching concept of 4D arrays are outlined in Section 2. Section 3 briefly describes a wavelet-based heuristic method. In Section 4, the results are examined with comparative and comprehensive analysis. The concluding remarks are laid out in Section 5.

Theory and design equations

The simplified beamforming network (BFN) of a 4D linear array consists of N isotropic radiators attached through rapid radio-frequency (RF) switches, is shown in Fig. 1. The corresponding array factor (AF) without any loss of generality can be given as [1]

$$AF(\theta, t) = e^{j(2\pi f_0)t} \sum_{n=1}^{N} I_n U_n(t) e^{jk(n-1)d\cos\theta} \tag{1}$$

where, I_n represents the excitation of the nth antenna, k is the propagation constant, d is considered as uniform element spacing, θ is the angle of impinging signals, f_0 is the central frequency with T_0 being the fundamental period, and $U_n(t)$ is the time modulation function.

Due to the periodic nature, $U_n(t)$ may be given as [1]

$$U_n(t) = \sum_{m=-\infty}^{\infty} a_{mn} e^{jm(2\pi f_p)t} \tag{2}$$

https://doi.org/10.1017/S175907872510158X Published online by Cambridge University Press

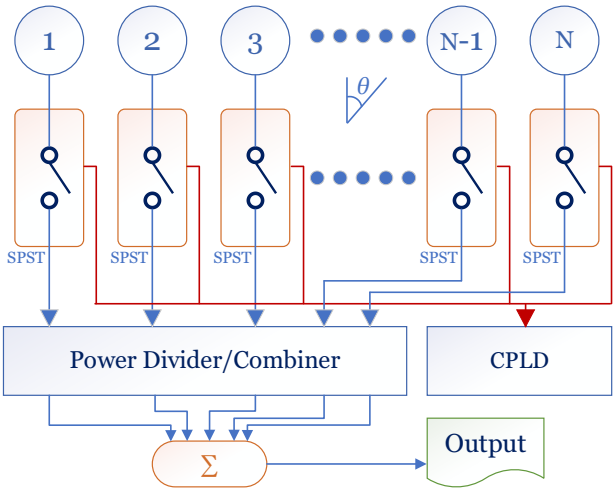


Figure 1. N-element fourth-dimensional (4D) linear antenna array with beamforming network (BFN).

The Fourier term of excitation (a_{mn}) for a particular radiating antenna (n^{th}) at pre-defined harmonic frequencies (m^{th}), automatically created due to modulation, can be given as [1]

$$a_{mn} = \frac{1}{T_p}\int_0^{T_p} U_n(t)\, e^{-jm(2\pi f_p)t}dt \tag{3}$$

Thus, the AF for uniformly excited ($I_n = 1$) 4D linear array may be expressed as [9]

$$AF(\theta, t) = \sum_{m=-\infty}^{\infty}\sum_{n=1}^{N} a_{mn}\left\{e^{jk(n-1)dcos\theta}\right\} e^{j2\pi(f_0+mf_p)t} \tag{4}$$

The corresponding AF for m^{th} order frequencies may be simplified as [9]

$$AF_m(\theta, t) = e^{j2\pi(f_0+mf_p)t}\sum_{n=1}^{N} a_{mn}e^{jk(n-1)dcos\theta} \tag{5}$$

The central pattern is generated at $m = 0$, and SRs are placed at multiple of modulation frequencies such as $m = \pm 1, \pm 2, \pm 3, \ldots, \pm\infty$. The directivity of the 4D array is [10]

$$Dir = \frac{|AF_0(\theta_0, \phi_0)|^2}{\frac{1}{4\pi}\sum_{m=-\infty}^{\infty}\int_0^{2\pi}\int_0^{\pi}|AF_m(\theta, \phi)|^2 sin\theta d\theta d\phi} \tag{6}$$

where the central pattern ($m = 0$) has placed at $\theta = \theta_0, \phi = \phi_0$ in a three-dimensional plane, and $AF_m(\theta, \phi)$ denotes the AF pattern at m^{th} harmonics.

Basic time modulation scheme

Considering its periodic character, the switching module $U_n(t)$ may be derived in different ways for different switching sequences. In order to achieve beamforming patterns, the method suggested here involves splitting and shifting of each separable pulses within a modulation period (T_p). Pulse splitting and shifted pulse, along with a general ON-OFF rectangular time scheme is shown in Fig. 2. $U_n(t)$ for the general one is expressed as [9]:

$$U_n(t) = \begin{cases} 1, & 0 \le \tau_n^1 \le t \le \tau_n^2 \le T_p \\ 0, & otherwise \end{cases} \tag{7}$$

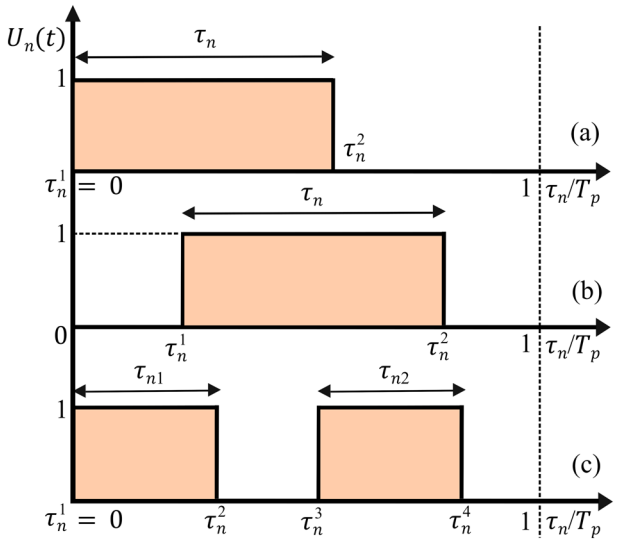


Figure 2. (a) simple pulse, (b) shifted pulse, (c) sub-sectioned pulse (pulse splitting).

The ON-time for n^{th} element is specified as τ_n within the modulation time T_p $(0 \le \tau_n \le T_p)$, and normalized ON-time is $\{\tau_n/T_p\}$. The element is turned ON initially (without shifting) as shown in Fig. 2(a) and the shifted pulse is given in Fig. 2(b). The shifted pulse starts at τ_n^1 and closes at τ_n^2 with a normalized ON-time $\{(\tau_n^2 - \tau_n^1)/T_p\}$. Taking uniform excitations $(I_n = 1)$ for each element of the array $(n = 1, 2, 3, \ldots N)$, a_{mn} can be determined as [9]

$$\begin{aligned}
a_{mn} &= \frac{1}{T_p}\int_{\tau_n^1}^{\tau_n^2} U_n(t)\, e^{-jm(2\pi f_p)t}\, dt \\
&= \frac{1}{T_p}\frac{1}{\{-jm(2\pi f_p)\}}\left[e^{-jm(2\pi f_p)t}\right]_{\tau_n^1}^{\tau_n^2} \\
&= \frac{1}{T_p}\frac{1}{\{-jm(2\pi f_p)\}}\left[e^{-jm(2\pi f_p)\tau_n^2} - e^{-jm(2\pi f_p)\tau_n^1}\right] \\
&= \frac{1}{T_p}\frac{j}{\{m(2\pi f_p)\}}\left[e^{-jm(2\pi f_p)\tau_n^1}\left\{e^{-jm(2\pi f_p)(\tau_n^2-\tau_n^1)} - 1\right\}\right] \\
&= \frac{1}{(1/f_p)}\frac{j}{\{m(2\pi f_p)\}}\left[e^{-jm(2\pi f_p)\tau_n^1}\right. \\
&\quad \left.\times\left\{e^{-jm\pi f_p(\tau_n^2-\tau_n^1)}\left(e^{-jm\pi f_p(\tau_n^2-\tau_n^1)} - e^{jm\pi f_p(\tau_n^2-\tau_n^1)}\right)\right\}\right] \\
&= \frac{j}{2\pi m}e^{-jm(2\pi f_p)\tau_n^1}e^{-jm\pi f_p(\tau_n^2-\tau_n^1)}\left[-2jsin\left\{m\pi f_p(\tau_n^2 - \tau_n^1)\right\}\right] \\
&= \frac{j(-2j)}{2\pi m}e^{-jm\pi f_p(2\tau_n^1+\tau_n^2-\tau_n^1)}\left[sin\left\{m\pi f_p(\tau_n^2 - \tau_n^1)\right\}\right] \\
&= \frac{1}{m\pi}\left[sin\left\{m\pi f_p(\tau_n^2 - \tau_n^1)\right\}\right]\, e^{-jm\pi f_p(\tau_n^1+\tau_n^2)} \\
&= f_p(\tau_n^2 - \tau_n^1)\frac{\left[sin\left\{m\pi f_p(\tau_n^2 - \tau_n^1)\right\}\right]}{\left[m\pi f_p(\tau_n^2 - \tau_n^1)\right]}e^{-jm\pi f_p(\tau_n^1+\tau_n^2)} \qquad (8)
\end{aligned}$$

$$= \frac{(\tau_n^2 - \tau_n^1)}{T_p}\left[sinc\left\{m\pi f_p(\tau_n^2 - \tau_n^1)\right\}\right]\, e^{-jm\pi f_p(\tau_n^1+\tau_n^2)} \tag{9}$$

Equation (9) represents the pulse shifted scheme of Fig. 2(b).

https://doi.org/10.1017/S175907872510158X Published online by Cambridge University Press

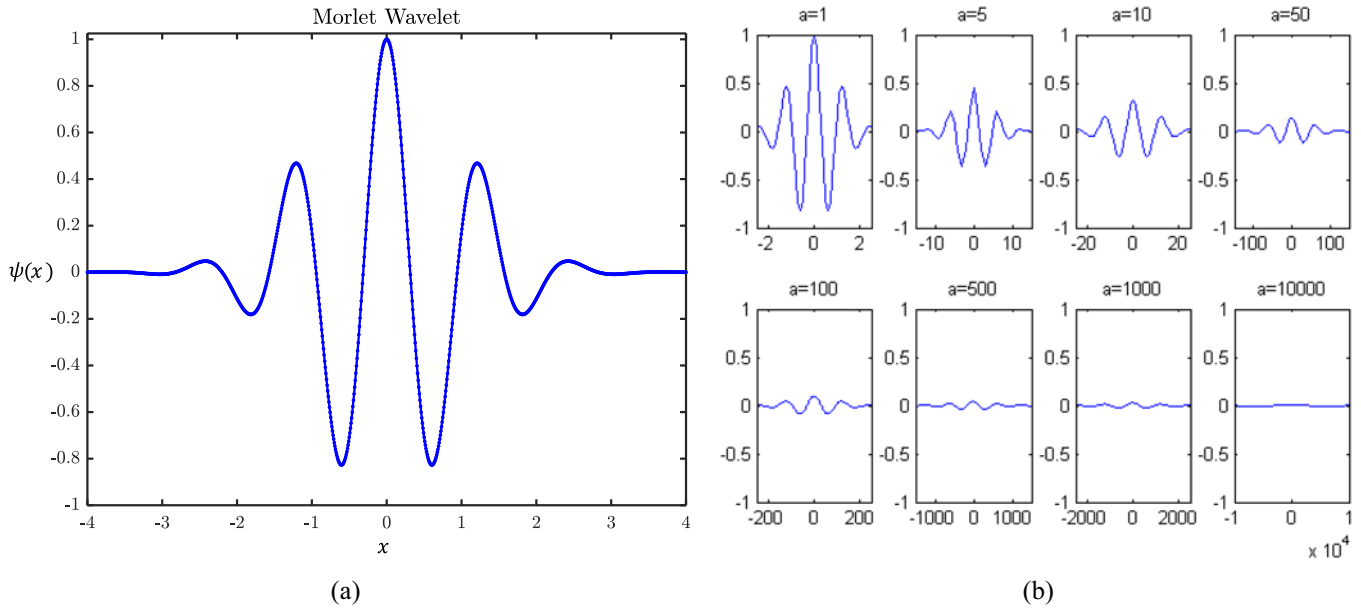


Figure 3. (a) morlet wavelet, (b) characteristics of morlet wavelet for different dilating parameter values [48].

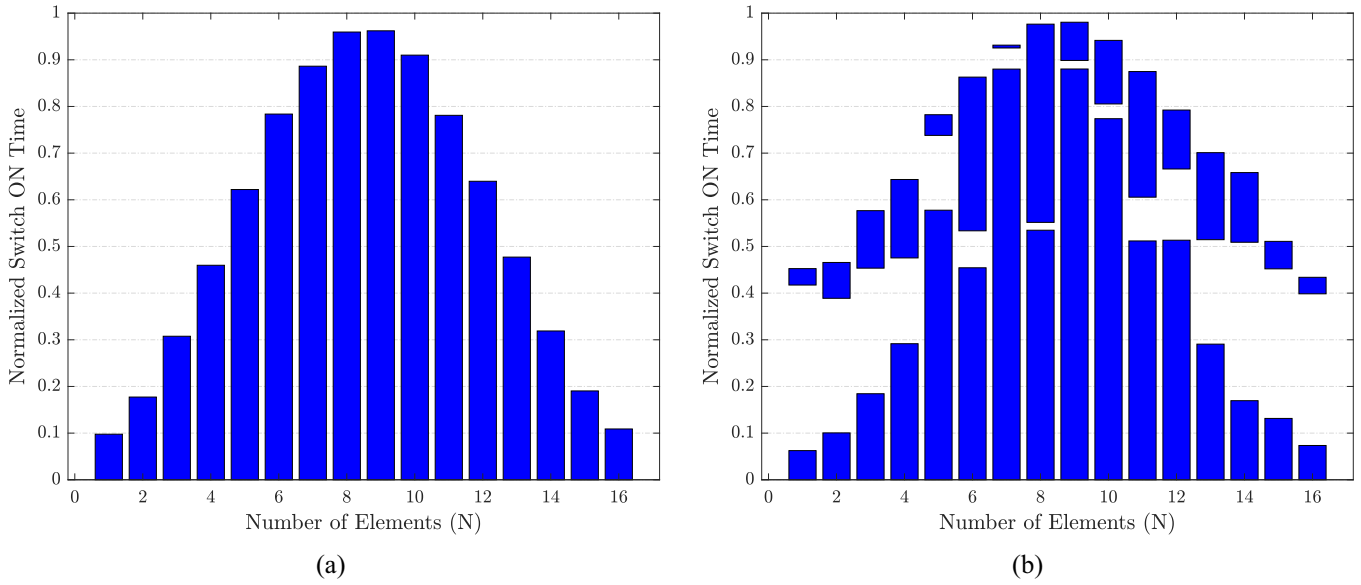


Figure 4. Optimal beamforming switch schemes (a) without and (b) with pulse splitting for 16-element array.

Switching with splitting pulses

To address a wide range of purposes, various switching mechanisms may be devised. Towards this purpose, a sub-sectioned splitting pulse scheme for n^{th} element is given in Fig. 2(c), where the ON-time of each antenna is split up into sub-sections having an OFF-time in between. The n^{th} element is turned ON at τ_n^1 ($\tau_n^1 = 0$) and stays ON up to τ_n^2 creating an ON-duration of τ_{n1} ($= \tau_n^2 - \tau_n^1$). Then, the antenna is turned OFF and stays OFF from τ_n^2 to τ_n^3 before going into the ON-state again for a duration of τ_{n2} ($= \tau_n^4 - \tau_n^3$). The modulation function $U_n(t)$ of the sub-pulse can be given as

$$U_n(t) = \begin{cases} 1, \ \tau_n^1 \le t \le \tau_n^2 \le T_p \text{ where } \tau_n^1 = 0 \\ 1, \ \tau_n^3 \le t \le \tau_n^4 \le T_p \text{ where } \tau_n^1 < \tau_n^3 \\ 0, \ \text{otherwise} \end{cases} \quad (10)$$

The a_{mn} for the sub-sectioned pulses may be expressed as

$$a_{mn} = \frac{(\tau_n^2 - \tau_n^1)}{T_p} \left[sinc \left\{ m\pi f_p (\tau_n^2 - \tau_n^1) \right\} \right] e^{-jm\pi f_p (\tau_n^1 + \tau_n^2)} + \frac{(\tau_n^4 - \tau_n^3)}{T_p} \left[sinc \left\{ m\pi f_p (\tau_n^4 - \tau_n^3) \right\} \right] e^{-jm\pi f_p (\tau_n^3 + \tau_n^4)} \quad (11)$$

These derivations indicate that modified switching schemes offer higher degrees of freedom (DoF) than the standard ON-OFF sequence. This added DoF can be effectively utilized by manipulating the harmonics without altering the central beam pattern. Splitting each time period into multiple time steps with different switch-ON instants, optimized switch-ON and switch-OFF intervals can be summarized from equation (11) as follows:

https://doi.org/10.1017/S175907872510158X Published online by Cambridge University Press

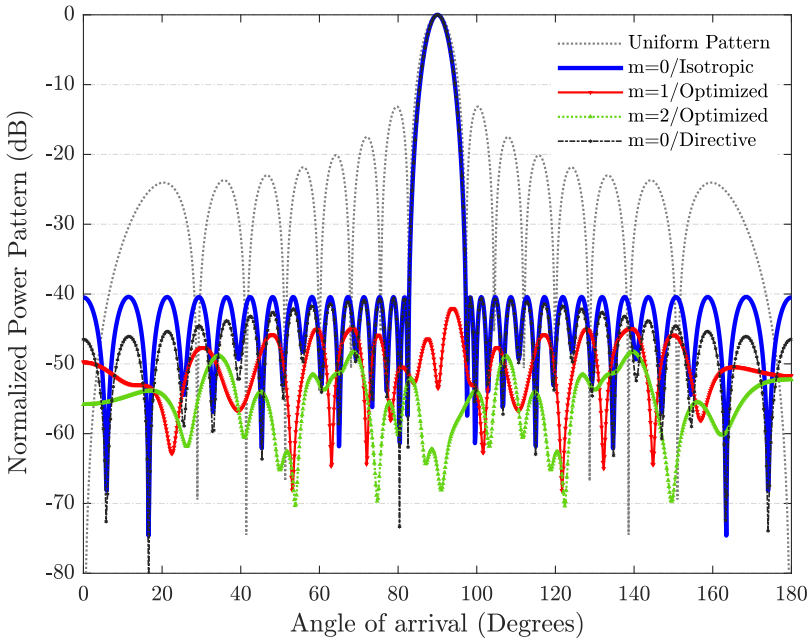


Figure 5. Optimal beamforming radiation patterns with reduced PSLL and sbls for 16-element array.

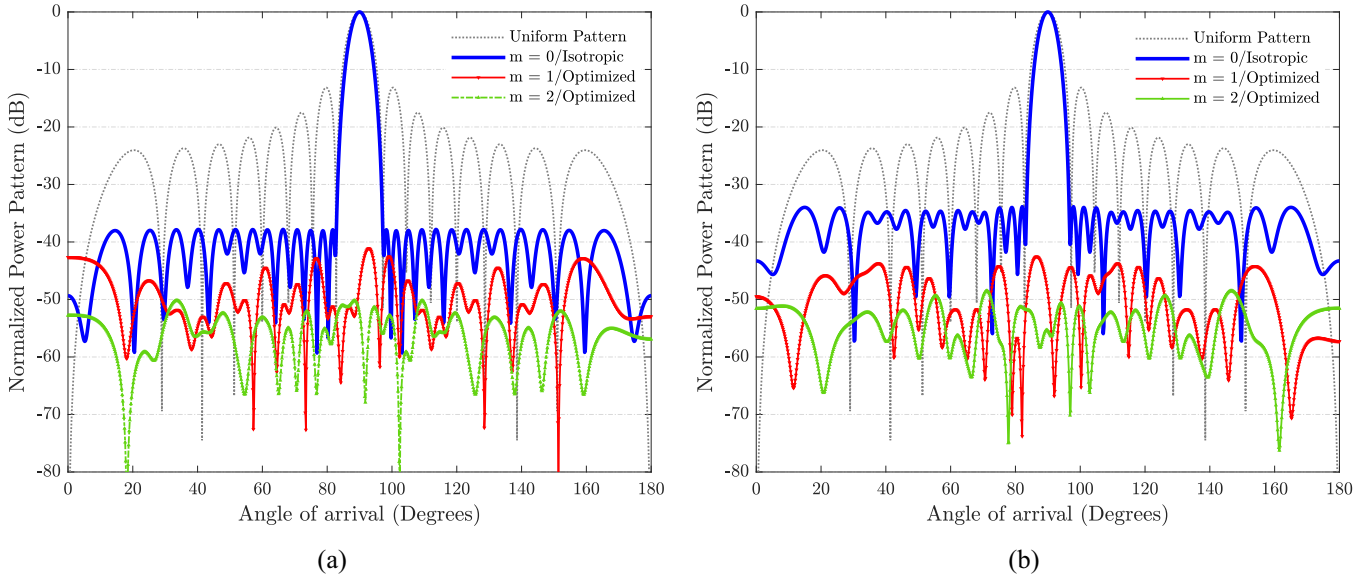


Figure 6. Beamforming radiation patterns 16-element array using (a) HPSO and (b) spso-based schemes.

$$a_{mn}^{r} = \sum_{r=1}^{s} \frac{(\tau_n^{r+1} - \tau_n^{r})}{T_p} \left[sinc\left\{ m\pi f_p \left(\tau_n^{r+1} - \tau_n^{r}\right)\right\}\right] e^{-jm\pi f_p(\tau_n^{r} + \tau_n^{r+1})} \tag{12}$$

Equation (12) represents splitting pulse shown in Fig. 2(c). Here, $r = 1$ represents only the shifting of pulses for each antenna, and $r > 1$ can be accounted for splitting of pulses into sub sections and shifting them with optimal time intervals between each sub-sectioned pulse. By taking $r = 0$, the generalized expression of a_{mn} for the mth harmonic at $m = 0$ can also be found from eqn. (12) as:

$$a_{mn} = \frac{\tau_n}{T_p} \left\{ sinc\left(m\pi f_p \tau_n\right)\right\} e^{-jm\pi f_p(\tau_n)} \tag{13}$$

where, $\tau_n = (\tau_n^2 - \tau_n^1)$ and the excitation coefficient of central pattern ($m = 0$) is given as: $a_{mn} = \{\tau_n / T_p\}$. This indicates that the central beam is not altered with splitting and shifted pulse, as it is mathematically related only to the switch-ON time of the antennas. But the SR patterns depend on switch-ON instants as well as the switch-ON time periods for beamforming.

Design equation for optimization

Therefore, it turns out that the sideband power losses can be suppressed by properly adjusting the values of the static excitations, as well as the durations and starting instants of the ON-time pulses. To further reduce the optimization burden and the control parameters, uniform amplitude is taken in to account. Then, using an iterative heuristic optimization approach, the switch-ON instants and the switch-ON time periods are tuned with the goal of minimizing the SLLs and SBLs of a specific cost function. Reduction in

https://doi.org/10.1017/S175907872510158X Published online by Cambridge University Press

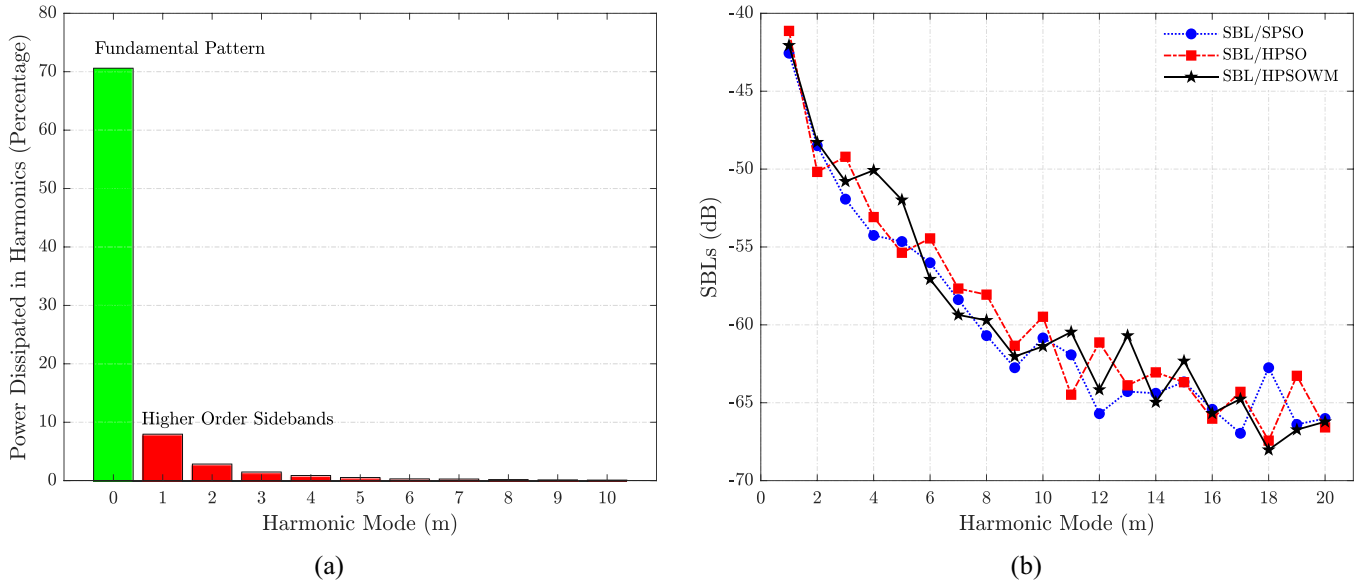


Figure 7. (a) power dissipated in main beam and sidebands with HPSOWM, (b) optimized higher-order sbls.

sideband power losses and interference rejection of the central pattern for beamforming may be targeted as a minimization problem. By optimizing the normalized ON-time periods of each antenna, the SLL of the main beam can be lowered. Sideband radiation power may be is averaged over the whole angular region by optimally shifting and splitting the ON-time pulses. The CF for the overall optimization process is designed as

$$\begin{aligned} \mathrm{CF} = & \left\{\psi^{SLL(i)}\left(\tau_n\right)\right\}\Big|_{f_0 \pm m f_p\,(m=0)} \\ & + \left\{\psi^{SBL(i)}\left(\tau_n, \tau_n^r\right)\right\}\Big|_{f_0 \pm m f_p\,(m=1,2,3,\ldots,\infty)} \end{aligned} \tag{14}$$

where, $\psi^{\mathrm{SLL}(i)} = \mathrm{H}\left[\mathrm{SLL_{REF}} - \mathrm{SLL_{OBS}}\right]\left(\left|\mathrm{SLL_{REF}} - \mathrm{SLL_{OBS}}\right|^2 / \left|\mathrm{SLL_{REF}}\right|^2\right)$, $\mathrm{SLL_{REF}}$ and $\mathrm{SLL_{OBS}}$ are the reference and observed SLLs respectively, $\psi^{SBL(i)}$ represents the minimization of all the higher SBLs, H[.] is the Heaviside unit step function, and i denotes the number of evolutions performed for the optimization process.

Heuristic optimization technique

Heuristic optimization algorithms are robust and adaptive in nature, and combines the exploration and exploitation strategies to investigate a solution space for optimum solutions [43]. Evolutionary optimizations have evolved as population-based metaheuristic search method motivated by natural phenomena for solving various real-world engineering problems, especially in the area of antenna array synthesis [44–46].

Standard particle swarm optimization

Particle swarm optimization (PSO) is a well-known, robust, and stochastic optimization tool based on the movement and intelligence of swarms [47]. Standard PSO (SPSO) has been demonstrated to be beneficial for a number of fields for optimizing challenging multidimensional discontinuous problems especially antenna design and pattern synthesis in electromagnetics [47]. SPSO models the sociological behaviour of bird flocking and fish schooling in multi-dimensional space. It takes into account a number of particles that collectively constitute a swarm. Each particle in the swarm traverses the solution space looking for the global best (g_{best}) while considering their individual or personal best (p_{best}) also at each iteration. The process continues by minimizing the distance between the present position of the particle and its personal best (p_{best}), as well as, the distance between the present position of a particle and the global best (g_{best}) as per the following equations:

$$\begin{aligned} v_j^p\left(i+1\right) = C_F.\Big\{ & w.v_j^p\left(i\right) + \varphi_1.rand_1.\left(p_{best_j}^{\ p} - s_j^p\left(i\right)\right) \\ & + \varphi_2.rand_2.\left(g_{best_j} - s_j^p\left(i\right)\right)\Big\} \end{aligned} \tag{15}$$

$$s_j^p\left(i+1\right) = s_j^p\left(i\right) + v_j^p\left(i+1\right) \tag{16}$$

Here, eqn. (15) and (16) are the velocity updating and position updating equations, respectively. The $v_j^p\left(i\right)$ is the velocity at i$^{\mathrm{th}}$ iteration, with $p = 1, 2, \ldots, \gamma$ being the number of particles in the swarm and $j = 1, 2, \ldots, \kappa$ being the dimension of the particle. The φ_1 and φ_2 in eqn. (15) represents the social and cognitive acceleration constants; w is the inertia weight factor; $s_j^p\left(i\right)$ is the present position of a particle in the search space; $rand_1$ and $rand_2$ are the random numbers in between 0 and 1. The C_F stands for the constriction factor which affects the stability analysis by ensuring no premature convergence, and mathematically represented in terms of acceleration constants as [48]:

$$C_F = \frac{2}{\left|2 - \varphi - \sqrt{\varphi^2 - 4\varphi}\right|} \tag{17}$$

Here, $\varphi = \varphi_1 + \varphi_2$ and $\varphi > 4$.

Hybrid PSO with wavelet mutation

Towards the near-optimal solution, SPSO typically encounters issues related to velocity updating despite working effectively in the beginning. If the particle's present state is coinciding with global best position, the particle will only move from its present state if its inertia weight and velocity are different from zero. The particles

https://doi.org/10.1017/S175907872510158X Published online by Cambridge University Press

https://doi.org/10.1017/S175907872510158X Published online by Cambridge University Press

Table 1. Numerical results for the proposed beamforming 4D array with optimized time schemes

Elements	Algorithms	**ON-Time Durations (τ_n/T_p)**	**Pulse Splitting Instants (τ'_n/T_p)**	**Spacing (λ)**	$PSLL_0$ (*dB*)	$PSBL_1$ (*dB*)	$PSBL_2$ (*dB*)	FNBW (*degree*)	Directivity (*dB*)
16	HPSOWM	0.0978 0.1774 0.3077 0.4598 0.6221 0.7838 0.8864 0.9596 0.9622 0.9101 0.7811 0.6398 0.4773 0.3190 0.1905 0.1090	0.4174 0.3890 0.4536 0.4755 0.7381 0.5336 0.9254 0.5516 0.8987 0.8055 0.6057 0.6661 0.5146 0.5091 0.4521 0.3986	0.75	−40.48	−42.60	−48.38	17.64	12.98
	HPSO	0.1127 0.2018 0.3023 0.4628 0.6057 0.7362 0.8685 0.9246 0.9384 0.8850 0.7937 0.6570 0.4831 0.3510 0.1992 0.1318	0.5223 0.4187 0.5024 0.6672 0.4499 0.6423 0.5767 0.7982 0.5706 0.5729 0.5176 0.4708 0.6556 0.5037 0.4773 0.4208	0.75	−37.81	−41.13	−50.18	17.88	12.03
	SPSO	0.1727 0.2420 0.3678 0.4766 0.6791 0.7723 0.9053 0.9825 0.9313 0.8966 0.8509 0.6679 0.5470 0.3872 0.2400 0.1443	0.4403 0.4131 0.4269 0.5340 0.5342 0.5519 0.6428 0.5854 0.5144 0.6800 0.6071 0.6397 0.5594 0.4044 0.5441 0.3628	0.75	−33.89	−42.56	−48.50	17.84	12.02
24	**HPSOWM**	**0.1045 0.1481 0.1974 0.3027 0.3959 0.4881 0.6190 0.7162 0.8069 0.8795 0.9232 0.9619 0.9370 0.9111 0.8633 0.7591 0.6749 0.5672 0.4694 0.3626 0.2524 0.1931 0.1103 0.0832**	**0.4496 0.4563 0.5299 0.4904 0.4857 0.6042 0.6062 0.6045 0.8224 0.6688 0.7207 0.5964 0.5779 0.6940 0.6984 0.4852 0.5477 0.4551 0.5079 0.5452 0.5607 0.4763 0.4783 0.3725**	**0.75**	**−41.35**	**−41.7**	**−47.62**	**11.88**	**13.71**
	HPSO	0.1615 0.2337 0.2426 0.3113 0.4240 0.4436 0.5446 0.5605 0.6862 0.6556 0.6701 0.7251 0.6666 0.6276 0.6780 0.5134 0.5006 0.4097 0.3691 0.2764 0.2197 0.1736 0.1115 0.1248	0.5044 0.4511 0.5174 0.4684 0.5166 0.4952 0.6830 0.5561 0.7773 0.6752 0.5496 0.5583 0.6296 0.5538 0.8223 0.4921 0.5273 0.5249 0.4296 0.4048 0.4370 0.4907 0.4078 0.3795	0.75	−32.34	−39.82	−45.55	10.44	13.32
	SPSO	0.1420 0.1974 0.2981 0.3374 0.5246 0.5058 0.5965 0.7229 0.7457 0.8321 0.8036 0.8340 0.8546 0.8105 0.7627 0.6905 0.5790 0.5727 0.4235 0.3636 0.2482 0.1688 0.1820 0.1671	0.4971 0.5566 0.4895 0.5266 0.5470 0.5119 0.6868 0.6352 0.7430 0.5686 0.7241 0.5096 0.9020 0.6562 0.7384 0.4969 0.5960 0.5147 0.5284 0.5141 0.4503 0.4415 0.4081 0.4556	0.75	−32.70	−42.41	−48.06	10.44	13.26
30	**HPSOWM**	**0.0666 0.1143 0.1436 0.1896 0.2587 0.3373 0.4129 0.4986 0.5831 0.6573 0.7177 0.7998 0.8536 0.8665 0.9036 0.8930 0.8883 0.8509 0.7830 0.7375 0.6847 0.5537 0.5116 0.4098 0.3430 0.2582 0.2055 0.1409 0.0934 0.0788**	**0.3880 0.4559 0.5151 0.4370 0.4736 0.4517 0.6212 0.5223 0.6235 0.4928 0.5959 0.5712 0.7017 0.4945 0.6980 0.5019 0.7099 0.6016 0.5433 0.5047 0.7820 0.6789 0.4294 0.5801 0.4972 0.4960 0.5527 0.5006 0.5097 0.3834**	**0.75**	**−42.43**	**−42.14**	**−44.15**	**9.72**	**14.91**
	HPSO	0.1118 0.2507 0.2702 0.3382 0.2861 0.4196 0.4548 0.5684 0.5555 0.7032 0.7080 0.7286 0.8805 0.8695 0.8160 0.8020 0.8807 0.7599 0.7016 0.7439 0.7413 0.6290 0.5314 0.5183 0.5430 0.2878 0.2976 0.2723 0.1613 0.2937	0.3818 0.4855 0.4958 0.5099 0.5687 0.4563 0.4929 0.6229 0.5877 0.6355 0.6977 0.5296 0.5070 0.5915 0.7109 0.5708 0.6082 0.5036 0.6116 0.4995 0.5748 0.5726 0.6355 0.5284 0.5524 0.5338 0.5228 0.4842 0.4269 0.4196	0.75	−30.17	−41.3	−48.41	7.56	14.85
	SPSO	0.2080 0.3965 0.4622 0.4419 0.6078 0.5646 0.4850 0.5894 0.8703 0.7703 0.8971 0.8449 0.9364 0.8807 0.9989 0.7851 0.9867 0.9659 0.8659 0.9581 0.5878 0.5423 0.8210 0.4419 0.6046 0.4811 0.1926 0.2991 0.2224 0.3029	0.5249 0.5267 0.5534 0.4974 0.5264 0.6016 0.5144 0.6551 0.4908 0.5414 0.6153 0.5147 0.7261 0.8876 0.8243 0.5007 0.6267 0.9586 0.6877 0.6929 0.6325 0.6793 0.6707 0.5781 0.5252 0.5302 0.3895 0.5192 0.5763 0.5155	0.75	−25.83	−41.95	−49.83	7.20	14.20

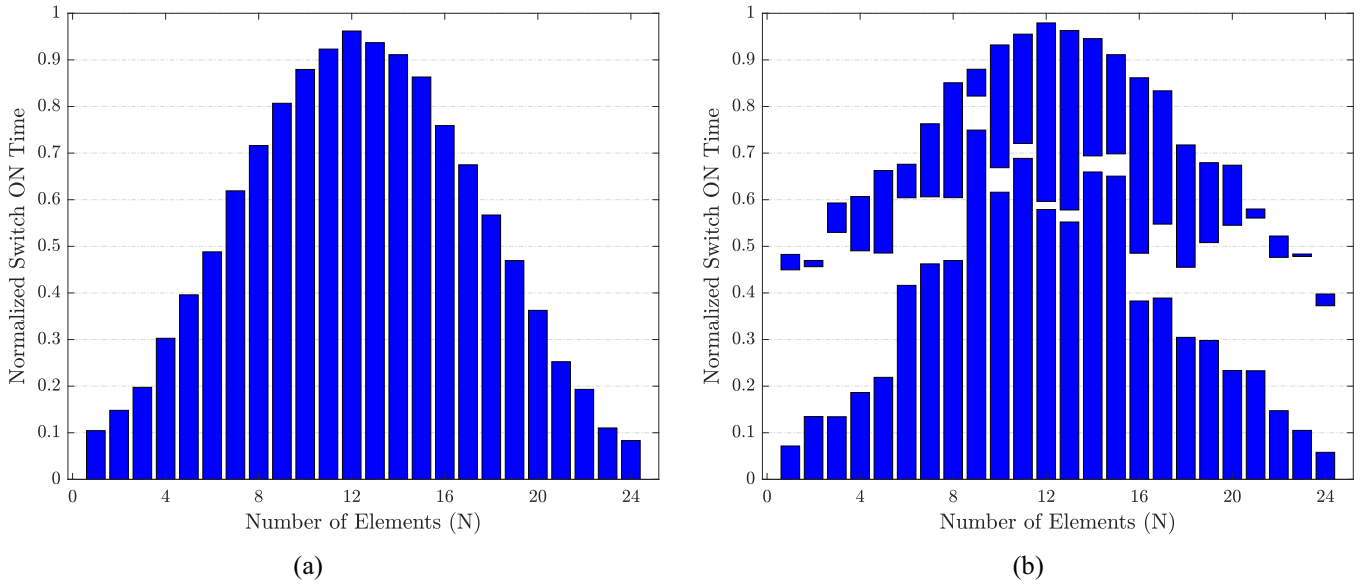


Figure 8. Optimal beamforming switch schemes (a) without and (b) with pulse splitting for 24-element array.

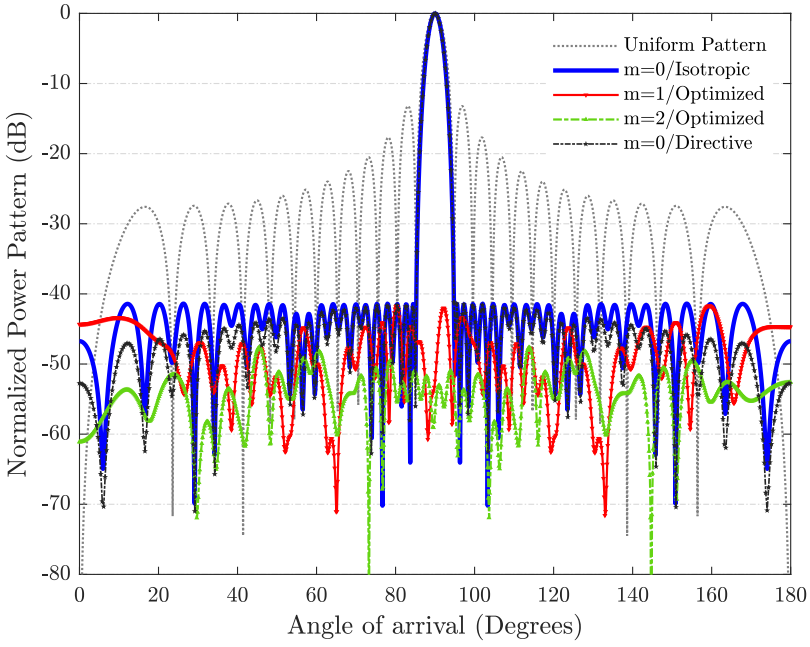


Figure 9. Optimal beamforming radiation patterns with reduced PSLL and sbls for 24-element array.

will stop moving if their velocities are near to zero, and they will catch up with the g_{best}, which may result in an early convergence and prevent future development by being stagnant at a particular position. To balance the global and local explorations, the inertia weight factor w may be chosen dynamically as [48]:

$$w = \left[w_{max} - \left\{ \left(\frac{w_{max} - w_{min}}{i_{max}} \right) * i \right\} \right] \tag{18}$$

Here, i_{max} presents the maximum iterations; and w is varied between the upper (w_{max}) and lower (w_{min}) limits in a range of [1,0.4]. The hybrid PSO (HPSO) is proposed by integrating the mutation operation of genetic algorithms [49] to break through the stagnation stages of SPSO as following:

$$mut\,(s_j) = \begin{cases} (s_j - k),\ r < 0 \\ (s_j + k),\ r \geq 0 \end{cases} \tag{19}$$

Here, s_j is the randomly chosen element of the particle from the swarm; r is a random number in between—1 and 1; k is randomly generated within $\left[0{,}0.1 * \left(par^j_{max} - par^j_{min}\right)\right]$; where par^j_{min} and par^j_{max} are the lower and upper limits of each particle, respectively. However, the mutation space in HPSO is limited by k. It might not be the best approach to always fix the size of the mutation space during the search. Rather, a dynamic mutation process that dynamically shrinks the mutation space along the search may be integrated. To implement this, a wavelet mutation (WM) approach is integrated with HPSO.

https://doi.org/10.1017/S175907872510158X Published online by Cambridge University Press

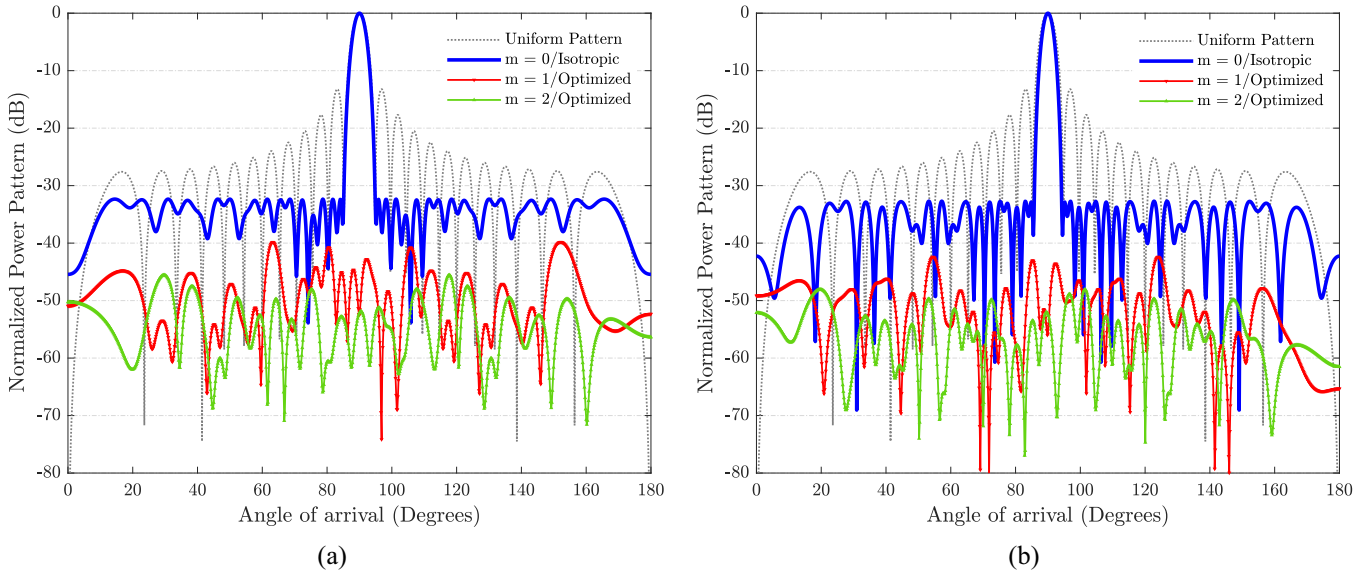


Figure 10. Beamforming radiation patterns 24-element array using (a) HPSO and (b) spso-based schemes.

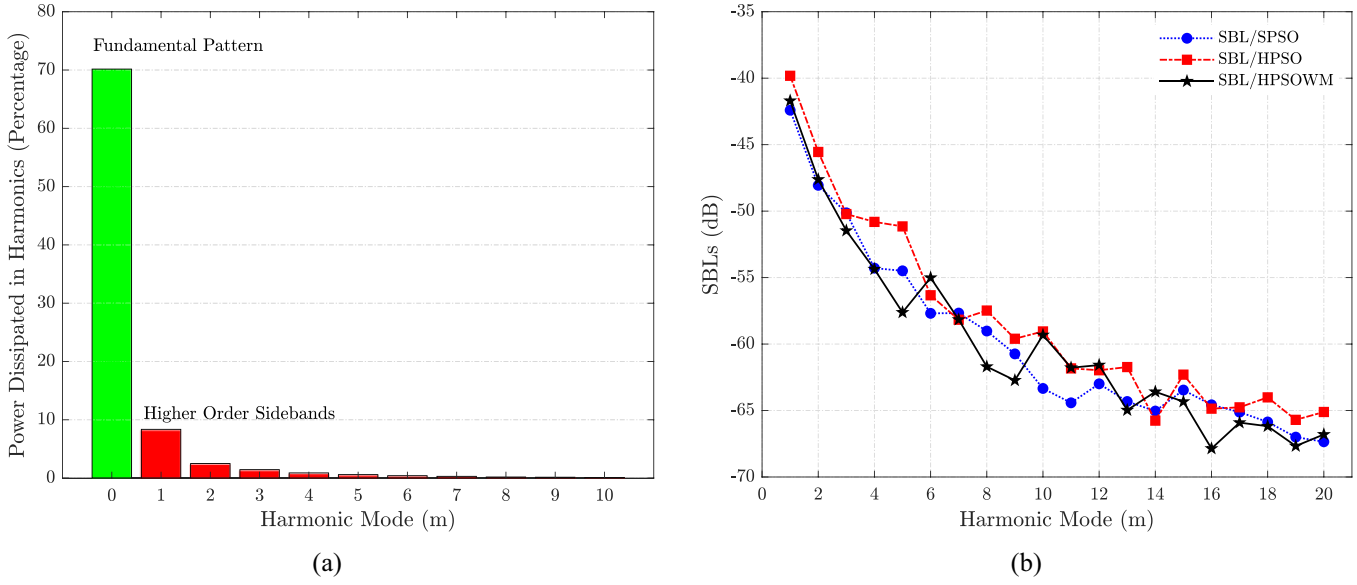


Figure 11. (a) power dissipated in main beam and sidebands with HPSOWM, (b) optimized higher-order sbls.

Basic wavelet theory

The translating and dilating oscillatory properties of some specific seismic signal may be modelled in to a continuous function $\psi(x)$ generally called as "*Morlet*" or "*mother wavelet*" if it satisfies the following properties [48]:

$$\text{Property 1}: \int_{-\infty}^{+\infty} \psi(x)\, dx = 0 \tag{20}$$

$$\text{Property 2}: \int_{-\infty}^{+\infty} |\psi(x)|^2 < \infty \tag{21}$$

It means that the total momentum of $\psi(x)$ is equal to zero, or the positive and negative momentum of $\psi(x)$ is equal to each other. Also, the continuous function $\psi(x)$ can be said finite and bounded. A typical "*Morlet wavelet*" is shown in Fig. 3(a), and may be represented mathematically as [48]

$$\psi(x) = e^{-x^2/2} \cos(5x) \tag{22}$$

For controlling the magnitude and position of the "*Morlet wavelet*", the continuous function $\psi(x)$ is extended as [48]

$$\psi_{a,b}(x) = \frac{1}{\sqrt{a}} \psi\left(\frac{x-b}{a}\right) \tag{23}$$

Here, a and b are the dilating and translating parameters, respectively. With $b = 0$, the amplitude scaled version of $\psi(x)$ can be derived. The scaled $\psi_{a,0}(x)$ for the different dilation properties are shown in Fig. 3(b), and can be represented mathematically as [48]

$$\psi_{a,0}(x) = \frac{1}{\sqrt{a}} \psi\left(\frac{x}{a}\right) \tag{24}$$

https://doi.org/10.1017/S175907872510158X Published online by Cambridge University Press

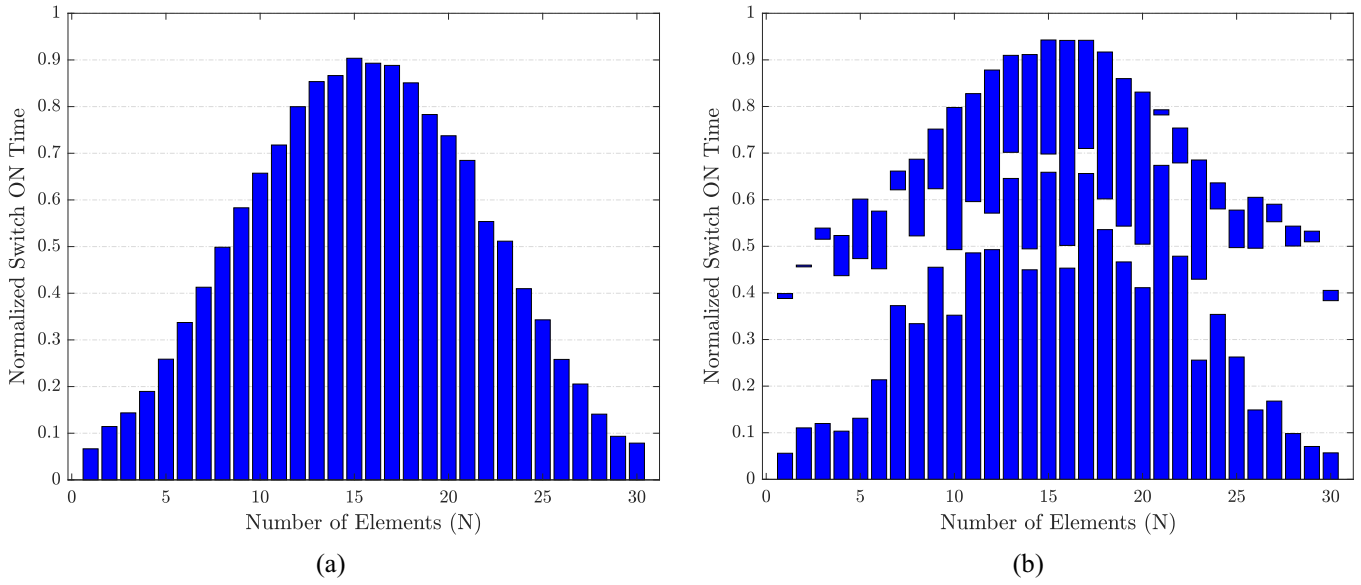


Figure 12. Optimal beamforming switch schemes (a) without and (b) with pulse splitting for 30-element array.

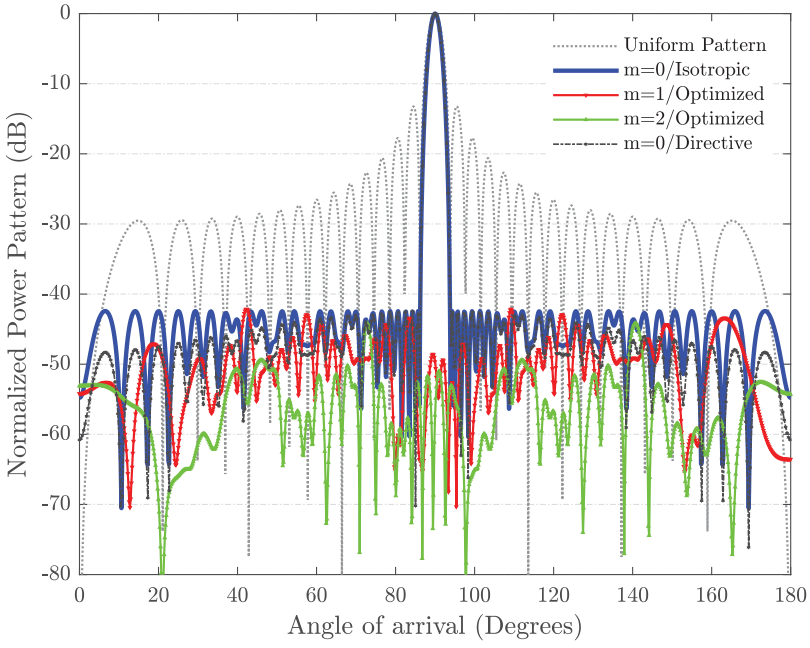


Figure 13. Optimal beamforming radiation patterns with reduced PSLL and sbls for 30-element array.

The amplitude can be scaled down by increasing the value of dilating parameter, and this property is utilized in the mutation process to enhance the search performance of the algorithm [48].

Operation of the WM

The wavelet-based mutation exhibits fine tuning by giving every element particle of the swarm a chance to mutate within a user-defined mutation probability $P_m \in [0,1]$. Thus, if the p^{th} particle is chosen and the element particle of the swarm $x_j^p(i)$ is selected randomly for mutation, the resultant particle can be given as [48]

$$\bar{x}_j^p(i) = \begin{cases} x_j^p(i) + \sigma.\left[par_{max}^j - x_j^p(i)\right] & if\ \sigma > 0 \\ x_j^p(i) + \sigma.\left[x_j^p(i) - par_{min}^j\right] & if\ \sigma \le 0 \end{cases} \quad (25)$$

Here, $\sigma = \psi_{a,0}(x) = \frac{1}{\sqrt{a}}\psi\left(\frac{x}{a}\right)$ and $\psi(x) = e^{\left(-\frac{x^2}{2}\right)}cos(5x)$. So, dilating parameter (σ) becomes

$$\sigma = \frac{1}{\sqrt{a}} e^{\left\{\left(-\frac{x}{a}\right)^2/2\right\}} cos\left\{5\left(\frac{x}{a}\right)\right\} \quad (26)$$

When σ is positive ($\sigma > 0$) and approaching to $+1$, the mutated particle element tends to have the maximum of $x_j^p(i)$. On the other hand, when σ is negative ($\sigma \le 0$) and approaching to—1, it has the minimum value of $x_j^p(i)$. The larger the value of $|\sigma|$, the searching space for fine tuning is large and vice-versa. According to the properties of mother wavelet, the sum of the positive and negative σ are equal when the sample is large. Thus, the positive and negative mutation is equal which provides a better solution stability. Further, the dilating parameter (a) can be expressed as

$$a = e^{-ln(g)*\left(1-\frac{i}{K}\right)^{\xi_{wm}}+ln(g)} \quad (27)$$

https://doi.org/10.1017/S175907872510158X Published online by Cambridge University Press

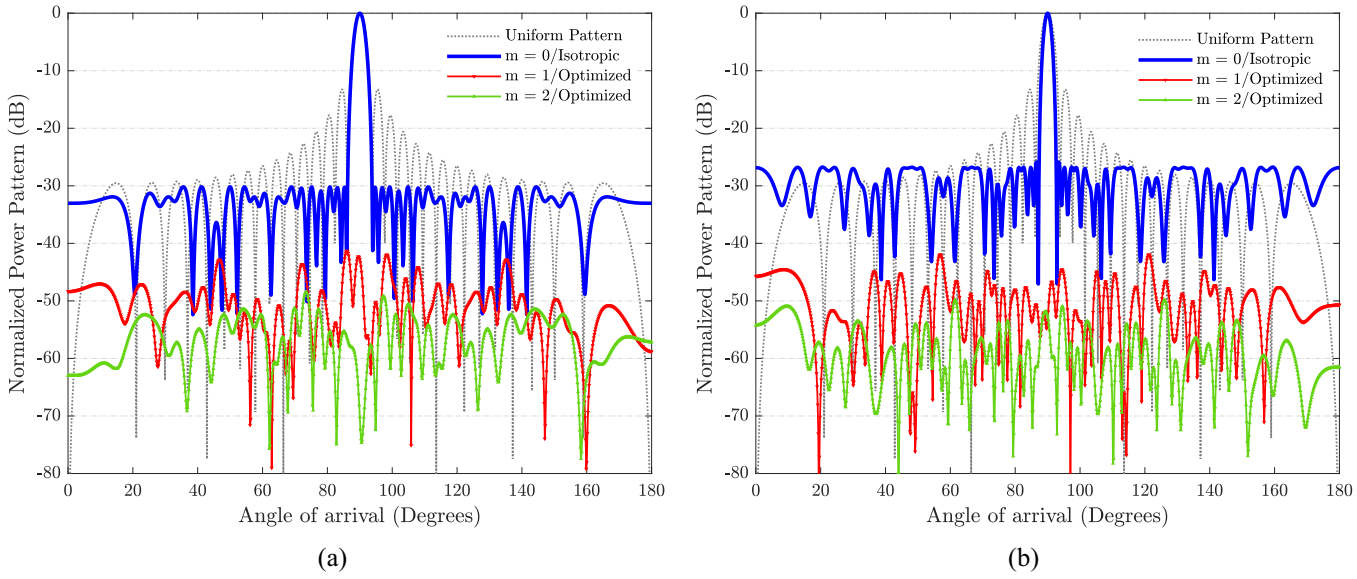


Figure 14. Beamforming radiation patterns 30-element array using (a) HPSO and (b) spso-based schemes.

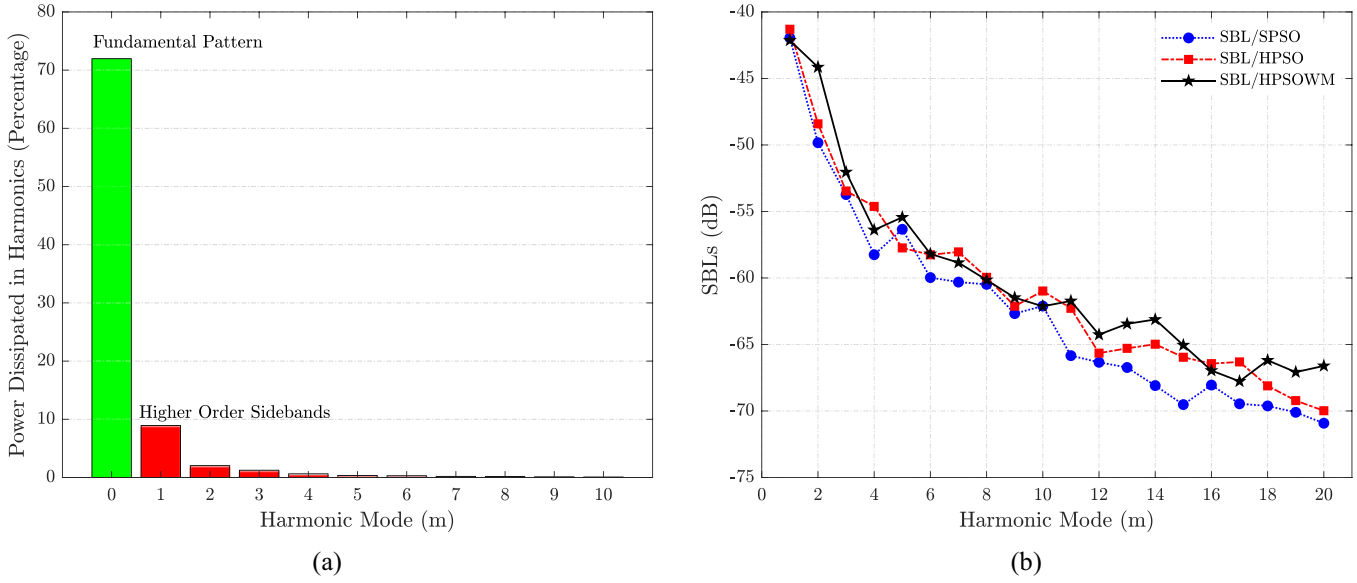


Figure 15. (a) power dissipated in main beam and sidebands with HPSOWM, (b) optimized higher-order sbls.

The dilating parameter (a) varies with $\left(\frac{i}{K}\right)$, where i stands for current evolution and K is the total number of evolutions. The monotonically increasing shape parameter is denoted by ξ_{wm} and g is the upper limit of the dilating parameter a [1,10000]. In HPSOWM, an optimal balance is projected between the exploitation of previously sampled regions in the search space and the exploration of new regions. An updated swarm is created after the WM operation, and the swarm will follow the same process over and over again until the termination criteria is reached.

Numerical data and analysis

This upcoming section discusses the numerical outcomes by a thorough examination of 16, 24, 30-element 4D linear arrays that have been developed, where the required objectives are achieved by combining a soft computing method with pulse control methodologies. The operational frequency (f_0) of the 4D linear arrays is 3 GHz with a modulation frequency (f_p) of 1 MHz. The properties of isophoric ($I_n = 1$) 16, 24, 30-element 4D linear arrays are: Peak SLLs = —13.15 dB,—13.21 dB,—13.24 dB; 3 dB beamwidths (HPBWs) = 6.48˚, 4.32˚, 3.60˚; beamwidth within the first nulls (FNBWs) = 14.4˚, 9.72˚, 7.56˚; and directivities = 12.04 dB, 13.80 dB, 14.77 dB; respectively. All the simulations are performed with MATLAB.

Beamforming with splitting pulses

An analysis of 4D linear arrays is investigated here in order to produce less-attenuating radiating beam patterns with sequentially lowered SLLs and SBLs. First, high-directive beamforming arrays with ultra-low SLLs are targeted, and then all the higher SBLs are

https://doi.org/10.1017/S175907872510158X Published online by Cambridge University Press

Table 2. Statistical *t_test* comparisons for the proposed HPSOWM with HPSO and SPSO for 16-element array

Comparing algorithms	*t_test* value	Degree of freedom (β)	Critical values of *t_test* for 99.99% Confidence Interval
HPSOWM/HPSO	5.826570660454678	39	3.323
HPSOWM/SPSO	6.557087984054862	36	3.347

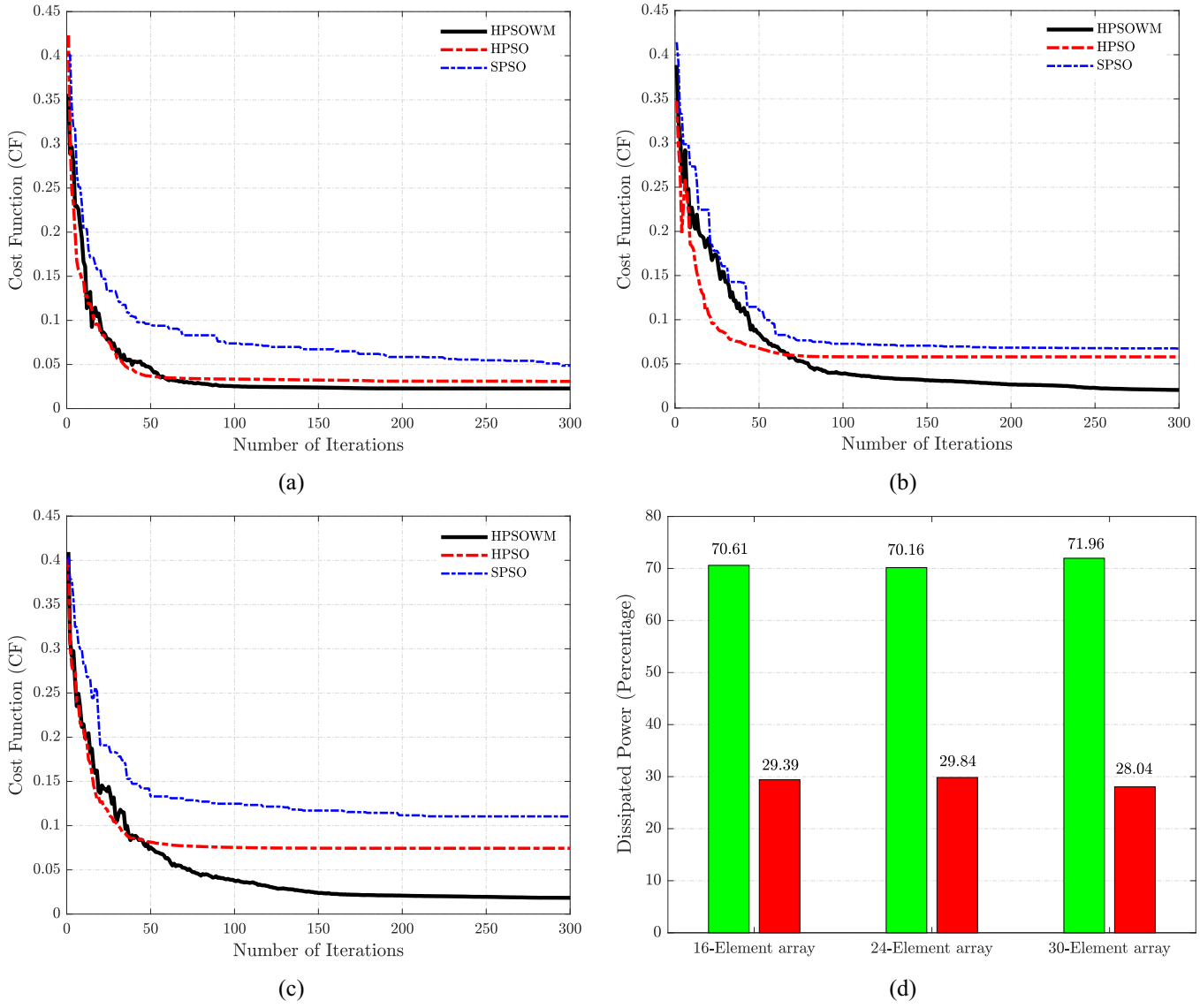


Figure 16. Convergence plots for (a) 16-element, (b) 24-element, (c), 30-element 4D array, and (d) comparison of used and unused power for hpsowm-based proposed 4D arrays.

minimized to reduce unwanted power loss. The aim is to design the optimal switching schemes by splitting the pulses within the pre-specified modulation period such that the SLL and the SBLs can be minimized to reduce the unwanted interference and the undesired power radiation in higher harmonics, respectively. The possible application of beamforming array is for directive point-to-point communication systems.

Beamforming with 16-element array

The 16-element beamforming 4D linear array is developed by aiming the objective of simultaneous SLL and SBLs reduction using pulse splitting. The ON-time and the pulse splitting instants of each array element are optimized, along with the uniform distance between each of them. The optimal outcomes are targeted by the proposed HPSOWM algorithm. The HPSOWM-based outcomes are also compared with HPSO and SPSO-based outcomes. To minimize the SBLs, the optimized ON-times of each antenna splits in two halves and shifted, so that the unwanted SRs can be outspread in a uniform way. The ON-times of the first pulse and the splitting instants of the second pulse are taken into account for optimization. Pulse splitting and shifting do not affect the central pattern, as central beam depends only upon the ON-time period. Thus, the central beam kept unchanged. The optimized beamforming switch schemes without and with pulse splitting derived by HPSOWM are presented in Fig. 4(a) and (b). The radiation pattern for point-to-point beamforming array is given in Fig. 5. Here, the uniform

https://doi.org/10.1017/S175907872510158X Published online by Cambridge University Press

Table 3. Comparison of efficiency of proposed array with execution time and optimized cost function values

Elements	Algorithms	Execution Time (Min)	Cost Function Value	Standard Deviation of CF	Array Efficiency (%)
16	HPSOWM	2.4038	0.022859	0.03012	70.61
	HPSO	2.9976	0.030835	0.05042	70.01
	SPSO	3.8972	0.048687	0.05732	68.72
24	**HPSOWM**	**3.1078**	**0.020461**	**0.02892**	**70.16**
	HPSO	4.5578	0.057925	0.05845	63.38
	SPSO	6.0985	0.067312	0.08764	52.43
30	**HPSOWM**	**4.1176**	**0.018379**	**0.02206**	**71.96**
	HPSO	6.0654	0.074395	0.09558	63.54
	SPSO	6.9895	0.110410	0.13167	61.96

pattern, as well as the optimized main beam pattern (f_0 at $m = 0$) with isotropic and directive elements are shown. The fixed inter-element spacing between each antenna is kept as 0.75λ. The radiation patterns obtained with HPSO and SPSO are also presented in Fig. 6(a) and (b), respectively. The proposed HPSOWM-based array is reported with a reduced PSLL of—40.48 dB compared to—13.15 dB PSLL of isophoric 4D array. HPSOWM-based pulse splitting approach also produces low SBLs, and the first two SBLs are reported as—42.6 dB and—48.38 dB. The FNBW and directivity reported for the proposed 4D array are 17.64° and 12.98 dB compared to 14.4° and 12.04 dB of isophoric array, respectively. The WM method is superior over the HPSO and SPSO methods as—37.81 dB and—33.89 dB PSLLs are obtained against—42.6 dB. The power at sideband is directly proportional to the nature of higher-order SBLs. The power generated at the main beam and first ten higher-order harmonics is shown in Fig. 7(a). In addition to that, the first twenty higher SBLs are also reported in Fig. 7(b) shows that the target objective of SLL and SBLs reduction are achieved simultaneously with the proposed 4D arrays. In the proposed beamforming array with HPSOWM, 70.61% power is utilized and 29.39% is wasted in higher-order harmonics compared to 70.01%, 29.99% and 68.72%, 31.28% obtained with HPSO and SPSO, respectively. The optimized numerical outcomes are shown in Table 1. The possible application of the proposed work is high-directive point-to-point communication system.

Beamforming with 24-element array

The 24-element beamforming 4D linear array is proposed here by aiming SLL and SBLs reduction simultaneously through pulse splitting. The ON-time and the pulse splitting instants of each array element are optimized. The optimal results are targeted by HPSOWM algorithm. The HPSOWM-based results are then compared with HPSO-based, SPSO-based and uniform 4D linear arrays. The optimized beamforming switch schemes without and with pulse splitting derived by HPSOWM are presented in Fig. 8(a) and (b). The radiation pattern for point-to-point beamforming array is given in Fig. 9. The fixed inter-element spacing of the array is kept as 0.75λ. The radiation patterns obtained with HPSO and SPSO are also shown in Fig. 10(a) and (b), respectively. The proposed HPSOWM-based array has a reduced PSLL of—41.35 dB compared to—13.21 dB of isophoric 4D array. HPSOWM-based pulse splitting approach also produces low SBLs, and the first two SBLs are reported as—41.7 dB and—47.62 dB. The FNBW and directivity reported for the proposed 4D array are 11.88° and 13.72 dB compared to 9.72° and 13.80 dB of the isophoric array, respectively. The WM method exhibits superiority over the HPSO and SPSO methods as—32.34 dB and—32.70 dB PSLLs are obtained against—41.35 dB. The power generated at the central beam and first ten higher-order harmonics is presented in Fig. 11(a). In addition to that, the first twenty higher SBLs are also reported in Fig. 11(b) shows that the objective of SLL and SBLs reduction are achieved simultaneously with the proposed 4D arrays. In the proposed beamforming array with HPSOWM, 70.16% power is utilized and 29.84% is wasted in higher-order harmonics compared to 63.38%, 36.62% and 52.43%, 47.57% obtained with HPSO and SPSO, respectively. The optimal numerical outcomes are shown in Table 1.

Beamforming with 30-element array

The 30-element beamforming 4D linear array is also proposed for the simultaneous SLL and SBLs reduction with pulse splitting. The optimal results are targeted by optimizing the ON-time and the pulse splitting instants of each antenna element using HPSOWM. The HPSOWM-based outcomes are compared with HPSO-based, SPSO-based and uniform 4D arrays. The optimized beamforming switch schemes without and with pulse splitting derived by HPSOWM are presented in Fig. 12(a) and (b). The radiation pattern for point-to-point beamforming array is given in Fig. 13. The fixed inter-element spacing of the array is kept as 0.75λ. The radiation patterns obtained with HPSO and SPSO are also shown in Fig. 14(a) and (b), respectively. The proposed HPSOWM-based array has a reduced PSLL of—42.43 dB compared to—13.24 dB of isophoric 4D array. HPSOWM-based pulse splitting approach also produces low SBLs and the first two SBLs are reported as—42.14 dB and—44.15 dB. The FNBW and directivity reported for the proposed 4D array are 9.72° and 14.91 dB compared to 7.56° and 14.77 dB of the isophoric array, respectively. The WM method exhibits superiority over the HPSO and SPSO methods as—30.17 dB and—25.83 dB PSLLs are obtained against—42.43 dB. The power generated at the central beam and first ten higher-order harmonics is presented in Fig. 15(a). In addition to that, the first twenty higher SBLs are also reported in Fig. 15(b) shows that the objective of SLL and SBLs reduction are achieved simultaneously with the proposed 4D arrays. In the proposed beamforming array with HPSOWM, 71.96% power is utilized and 28.04% is dissipated in higher-order harmonics compared to 63.54%, 36.46% and 61.96%, 28.04% obtained with HPSO and SPSO, respectively. The optimal numerical outcomes are shown in Table 1.

https://doi.org/10.1017/S175907872510158X Published online by Cambridge University Press

Table 4. Comparison of the proposed hpsowm-based outcomes with other works for 16-element array

References	$PSLL_0$ (*dB*)	$PSBL_1$ (*dB*)	$PSBL_2$ (*dB*)	Power Used (%)
Reference [8]	−30.00	−27.80	Na	Na
Reference [17]	−30.00	−19.50	−21.70	Na
Reference [51]	−25.50	−24.60	Na	Na
Reference [52]	−30.00	−25.53	−25.01	Na
Reference [53]	−30.00	−22.51	Na	Na
Reference [54]	−39.60	−29.90	Na	Na
Reference [55]	−31.90	−21.80	Na	Na
Reference [46]	−38.67	−24.98	−32.64	46.79
Reference [46]	−40.41	−24.96	−32.64	46.92
Reference [56]	−30.00	−35.98	Na	Na
Proposed (This work)	**−40.48**	**−42.60**	**−48.38**	**70.61**

Statistical test and comparison

To confirm the superiority of the WM method over HPSO and SPSO, two independents statistical *t_test* analysis is performed for the optimization problem in hand. Assuming unequal variances or standard deviations ($\sigma_1^2 \neq \sigma_2^2$) for a population, the test statistics may be calculated as [50]

$$t_{test} = \frac{\bar{\alpha}_{22} - \bar{\alpha}_{11}}{\sqrt{\left(\frac{\sigma_1^2}{n_A}\right) + \left(\frac{\sigma_2^2}{n_B}\right)}} \tag{28}$$

The degree of freedom (DoF) may be calculated as [50]

$$\beta = \frac{\left(\frac{\sigma_1^2}{n_A} + \frac{\sigma_2^2}{n_B}\right)^2}{\left\{\frac{\left(\frac{\sigma_1^2}{n_A}\right)^2}{(n_A - 1)} + \frac{\left(\frac{\sigma_2^2}{n_B}\right)^2}{(n_B - 1)}\right\}} \tag{29}$$

where, $\bar{\alpha}_{11}$ and $\bar{\alpha}_{22}$ are the means; σ_1 and σ_2 are the standard deviations; and n_A, n_B are the number of sample sizes considered for comparing the proposed algorithm with others. By considering $n_A = n_B$ for the 16-element 4D linear array, the *t_test* values obtained for different DoFs (β) comparing HPSOWM with HPSO and SPSO are presented in Table 2. The *t_test* values obtained are greater than the critical value [50], and that ensures the existence of an indicative deviation in HPSOWM's performance over HPSO and SPSO with 99.9% confidence.

The convergence plots of each method for the proposed 16, 24, and 30-element 4D linear arrays are shown in Fig. 16(a), (b), and (c), respectively. A comparison of used and wasted power for the HPSOWM-based proposed arrays is reported in Fig. 16(d). Comparison of efficiencies of the proposed arrays with execution time and optimized cost function values are reported in Table 3. Apart from all these statistical comparisons, the proposed array is also compared with other state of the art results, and presented in Table 4. The WM-based results show better performance in terms of array radiation properties compared to all the already reported works. Hence, a conclusion can be drawn that the proposed method is very well-suited for high-directive, secure point-to-point communication systems.

Conclusion

The adaptive radiation characteristics of fourth-dimensional (4D) linear antenna arrays have been explored in this article for beamforming applications. The point-to-point wireless communication system requires efficient, well-controlled, and optimized radiations patterns in specific directions. **Contributions**: The proposed array has achieved the target of ultra-low sidelobes beneficial for highly directive wireless transmission and reception. Simultaneously, the sideband levels (SBLs) have been reduced to minimize power distortion. The optimality of the array has further enhanced by introducing a hybrid particle swarm optimizer with wavelet-based mutation approach. The problems in hand are formulated in a single-objective cost function (CF) to optimize the beamforming network (BFN) consists of optimal ON-time duration and ON-time instances of the splitting pulses. The optimal switching sequences have been derived for three sets of linear 4D arrays by considering the target sidelobe below—40 dB. The inherent limitation of time-modulation, i.e., the formation of sidelobes at the multiple of harmonic frequencies have also been taken care of by proposing efficient pulse splitting techniques for all the arrays. The detailed comparison of the proposed array with simple PSO and hybrid PSO-based 4D arrays have also been reported which shows the effectiveness of the newly adopted mutation technique inspired by Morlet wavelets. **Benefits**: The targets have been attained with a reduction in SLL and SBLs below—40.48,—42.6 and—48.38 dB. The optimally splitting pulses-based single BFN also eliminates the implementational complexities. The power calculation has also shown that the arrays utilized more than 70% power in the main beam which indicates good beamforming performances for all three sets of arrays. Furthermore, the investigation of other reported works in this domain have also been carried over to compare the proposed array antenna. The comparison shown for 16-element array establishes the superiority of the proposed research as more than—40 dB SLL and SBLs compared to around—35 dB SLL and SBLs of the best-reported literature. Finally, it can be concluded that all the three sets of arrays with reduced sidelobes and sidebands are applicable for directive wireless signal transmission or reception, and can further be explored in near future for more advanced applications.

Data Availability Statement. No new data were created or analyzed during this study. Data sharing is not applicable to this article.

https://doi.org/10.1017/S175907872510158X Published online by Cambridge University Press

Competing interests. The authors declare that they have no known competing financial interests or personal relationships that could have appeared to influence the work reported in this paper.

References

1. **Rocca P, Yang F, Poli L and Yang S** (2019). Time-modulated array antennas – Theory, techniques, and applications. *Journal of Electromagnetic Waves and Applications* **33**, 1503–1531.
2. **Shanks HE and Bickmore RW** (1959). Four-Dimensional Electromagnetic Radiators. *Canadian Journal of Physics* **37**, 263–275.
3. **Shanks H** (1961). A new technique for electronic scanning. *IRE Transactions on Antennas and Propagation* **9**, 162–166.
4. **Kummer W, Villeneuve A, Fong T and Terrio F** (1963). Ultra-low sidelobes from time-modulated arrays. *IEEE Transactions on Antennas and Propagation* **11**, 633–639.
5. **Bregains JC, Fondevila-Gomez J, Franceschetti G and Ares F** (2008). Signal radiation and power losses of time-modulated arrays. *IEEE Transactions on Antennas and Propagation* **56**, 1799–1804.
6. **Yang S, Gan YB and Qing A** (2002). Sideband suppression in time-modulated linear arrays by the differential evolution algorithm. *IEEE Antennas and Wireless Propagation Letters* **1**, 173–175.
7. **Poli L, Rocca P, Manica L and Massa A** (2010). Handling sideband radiations in time-modulated arrays through particle swarm optimization. *IEEE Transactions on Antennas and Propagation* **58**, 1408–1411.
8. **Zhu Q, Yang S, Zheng L and Nie Z** (2012). Design of a low sidelobe time modulated linear array with uniform amplitude and sub-sectional optimized time steps. *IEEE Transactions on Antennas and Propagation* **60**, 4436–4439.
9. **Chakraborty A, Ram G and Mandal D** (2020). Optimal Pulse Shifting in Timed Antenna Array for Simultaneous Reduction of Sidelobe and Sideband Level. *IEEE Access* **8**, 131063–131075.
10. **Chakraborty A, Ram G and Mandal D** (2022). Time-modulated linear array synthesis with optimal time schemes for the simultaneous suppression of sidelobe and sidebands. *International Journal of Microwave and Wireless Technologies* **14**, 768–780.
11. **Tennant A and Chambers B** (2007). A two-element time-modulated array with direction-finding properties. *IEEE Antennas and Wireless Propagation Letters* **6**, 64–65.
12. **Li G, Yang S, Chen Y and Nie Z-P** (2009). A novel electronic beam steering technique in time modulated antenna array. *Progress In Electromagnetics Research* **97**, 391–405.
13. **Gang L, Yang S and Nie Z** (2010). Direction of arrival estimation in time modulated linear arrays with unidirectional phase center motion. *IEEE Transactions on Antennas and Propagation* **58**, 1105–1111.
14. **Poli L, Rocca P, Oliveri G and Massa A** (2011). Harmonic beamforming in time-modulated linear arrays. *IEEE Transactions on Antennas and Propagation* **59**, 2538–2545.
15. **Chakraborty A, Ram G and Mandal D** (2023). Phase center motion-based time modulated arrays with preprocessed time schemes for selective harmonic beamforming in B5G communication systems. *Trans Emerging Tel Tech* **34**, e4754.
16. **Chakraborty A, Ram G and Mandal D** (2022) Power pattern synthesis of a moving phase center time modulated antenna array using symmetrically and asymmetrically positioned time schemes. *International Journal of RF and Microwave Computer-Aided Engineering* 32.
17. **Poli L, Rocca P, Manica L and Massa A** (2010). Pattern synthesis in time-modulated linear arrays through pulse shifting. *IET Microwaves, Antennas & Propagation* **4**, 1157–1164.
18. **Poli L, Moriyama T and Rocca P** (2014). Pulse splitting for harmonic beamforming in time-modulated linear arrays. *International Journal of Antennas and Propagation* **2014**, 1–9.
19. **Poddar S, Paul P, Chakraborty A, Ram G and Mandal D** (2022). Design optimization of linear arrays and time-modulated antenna arrays using meta-heuristics approach. *International Journal of Numerical Modelling* **35**, e3010.
20. **Chakraborty A, Ram G and Mandal D** (2021). Pattern synthesis of timed antenna array with the exploitation and suppression of harmonic radiation. *International Journal of Communication* **34**, e4727.
21. **Chakraborty A, Saxena RS, Verma A, Juyal A, Gupta S, Singh I, Ram G and Mandal D** (2024). Multi-pattern synthesis in fourth-dimensional antenna arrays using BGM-based quasi-Newton memetic optimization method. *International Journal of Microwave and Wireless Technologies* **16**, 284–294.
22. **Chakraborty A, Ram G and Mandal D** (2023). Time modulation based unconventional phased antenna arrays for monopulse and multifunction radar systems. *Int J Numerical Modelling* **36**, e3074.
23. **Tong Y and Tennant A** (2010). Simultaneous control of sidelobe level and harmonic beam steering in time-modulated linear arrays. *Electronics Letters* **46**, 200–202.
24. **Chakraborty A, Ram G and Mandal D** (2021) Multibeam steered pattern synthesis in time-modulated antenna array with controlled harmonic radiation. *International Journal of RF and Microwave Computer-Aided Engineering* 31.
25. **Chakraborty A, Ram G and Mandal D** (2021). Time-modulated multi-beam steered antenna array synthesis with optimally designed switching sequence. *International Journal of Communication* **34**, e4828.
26. **Chakraborty A, Singh I, Gupta S, Ram G and Mandal D** (2023). Sideband power control in Time-Modulated antenna arrays for bidirectional harmonic beamforming and beam scanning. *AEU - International Journal of Electronics and Communications* **170**, 154788.
27. **Maneiro-Catoira R, Brégains J, García-Naya JA and Castedo L** (2022). Dual-beam steerable TMAs Combining AM and PM Switched Time-Modulation. *Sensors* **22**, 1399.
28. **Ram G and Mandal D** (2024). TMLAA for automatic harmonic beam steering toward user-defined direction using black hole mechanics optimization. *IEEE Transactions on Cognitive Communications and Networking* **10**, 1386–1397.
29. **Ma Y, Miao C, Li Y-H and Wu W** (2021). A partition-based method for harmonic beamforming of time-modulated planar array. *IEEE Transactions on Antennas and Propagation* **69**, 2112–2121.
30. **Li H, Chen Y and Yang S** (2022). Directional Modulation in Time-Modulated Array with a Novel Pseudorandom Ascending Phase Time Sequence. *IEEE Transactions on Microwave Theory and Techniques* **70**, 3319–3328.
31. **Dong X, Li H, Tan J, Hu J and Jiang Y** (2021). A PSO-CVX algorithm of sum and difference beam patterns for time-modulated antenna array. *International Journal of Antennas and Propagation* **2021**, 1–9.
32. **Chen K, Yang S, Chen Y, Qu S-W and Hu J** (2021). Hybrid directional modulation and beamforming for physical layer security improvement through 4-D antenna arrays. *IEEE Transactions on Antennas and Propagation* **69**, 5903–5912.
33. **Qu C, Chen K, Long W, Chen Y, Qu S-W, Hu J and Yang SA** (2022). A vector modulation approach for secure communications based on 4-D antenna arrays. *IEEE Transactions on Antennas and Propagation* **70**, 3723–3732.
34. **Suneel Varma D, Ram G and Arun Kumar G** (2023). Time-modulated multi-tone antenna array for wireless information and power transfer. *International Journal of Communication* **36**, e5419.
35. **Reyna A, Panduro MA, Romero G, Villanueva J, Rivera FF and Méndez AL** (2014). Two-dimensional time-domain antenna arrays for optimum steerable energy pattern with low side lobes. *International Journal of Antennas and Propagation* **2014**, 1–12.
36. **Reyna A, Panduro MA, Méndez AL and Romero G** (2016). Timed arrays of spiral antennas for circularly polarised UWB scanned patterns with low side lobes. *IET Microwaves, Antennas & Propagation* **10**, 587–593.
37. **Medina Z, Reyna A, Panduro MA and Elizarraras O** (2019). Dual-band performance evaluation of time-modulated circular geometry array with microstrip-fed slot antennas. *IEEE Access* **7**, 28625–28634.
38. **Ram G, Kar R and Mandal D** (2020). Control parameter based comparative study of radiation properties of TMCCAA and TMHSCAA. *Scientia Iranica* **0**, 0–0.

https://doi.org/10.1017/S175907872510158X Published online by Cambridge University Press

39. **Reyna Maldonado A, Panduro MA, Del Rio Bocio C and Mendez AL** (2013). Design of concentric ring antenna array for a reconfigurable isoflux pattern. *Journal of Electromagnetic Waves and Applications* **27**, 1483–1495.
40. **Jiménez DA, Reyna A, Panduro MA, Del Rio C, Ram G and Balderas L** (2020). UAVs-based antenna arrays using time modulation. *Telecommunication Systems* **74**, 113–127.
41. **Maldonado G, Maldonado AR, Balderas LI and Panduro MA** (2022). Time-modulated antenna arrays for ultra-wideband 5G applications. *Micromachines* **13**, 2233.
42. **Varma DS, Ram G and Arun Kumar G** (2023). Time-Modulated arrays: A review. *IETE Technical Review* **40**, 136–151.
43. **Del Ser J, Osaba E, Molina D, Yang X-S, Salcedo-Sanz S, Camacho D, Das S, Suganthan PN, Coello CA and Herrera F** (2019). Bio-inspired computation: Where we stand and what's next. *Swarm and Evolutionary Computation* **48**, 220–250.
44. **Sharaqa A and Dib N** (2014). Design of linear and elliptical antenna arrays using biogeography based optimization. *Arabian Journal for Science and Engineering* **39**, 2929–2939.
45. **Das A, Mandal D, Ghoshal SP and Kar R** (2019). A heuristic approach to design linear and circular antenna array for side lobe reduction. *Iran J Sci Technol Trans Electr Eng* **43**, 67–76.
46. **Ram G, Mandal D, Kar R and Ghoshal SP** (2016). Improvement in various radiation characteristics of time modulated linear antenna arrays using evolutionary algorithms. *Journal of Experimental & Theoretical Artificial Intelligence* **28**, 151–180.
47. **Robinson J and Rahmat-Samii Y** (2004). Particle swarm optimization in electromagnetics. *IEEE Transactions on Antennas and Propagation* **52**, 397–407.
48. **Ling SH, Iu HHC, Chan KY, Lam HK, Yeung BCW and Leung FH** (2008). Hybrid particle swarm optimization with wavelet mutation and its industrial applications. *IEEE Trans Syst, Man, Cybern B* **38**, 743–763.
49. **Weile DS and Michielssen E** (1997). Genetic algorithm optimization applied to electromagnetics: A review. *IEEE Transactions on Antennas and Propagation* **45**, 343–353.
50. **Scott JF, Walpole RE and Myers RH** (1973). Probability and statistics for engineers and scientists. *The Mathematical Gazette* **57**, 148.
51. **Yang S, Gan YB, Qing A and Tan PK** (2005). Design of a uniform amplitude time modulated linear array with optimized time sequences. *IEEE Transactions on Antennas and Propagation* **53**, 2337–2339.
52. **Chen J, Liang X, He C, Fan H, Zhu W, Geng J and Jin R** (2018). Instantaneous gain optimization in time modulated array using reconfigurable power divide/combiner. *IEEE Antennas and Wireless Propagation Letters* **17**, 530–533.
53. **Aksoy E and Afacan E** (2011) Sideband level suppression improvement via splitting pulses in time modulated arrays under static fundamental radiation. *PIERS Proceedings*.
54. **Yang S, Chen Y and Nie Z-P** (2009). Simulation of time modulated linear antenna arrays using the FDTD method. *Progress In Electromagnetics Research* **98**, 175–190.
55. **Zhu Q, Yang S, Zheng L and Nie Z** (2011). A pattern synthesis approach in four-dimensional antenna arrays with practical element models. *Journal of Electromagnetic Waves and Applications* **25**, 2274–2286.
56. **He C, Yu H, Liang X, Geng J and Jin R** (2015). Sideband radiation level suppression in time-modulated array by nonuniform period modulation. *IEEE Antennas and Wireless Propagation Letters* **14**, 606–609.

https://doi.org/10.1017/S175907872510158X Published online by Cambridge University Press